JOINT EUROPEAN TORUS

JET–P(92)42

M.R. O'Brien, M. Cox, C.D. Warrick, F.S. Zaitsev
and JET Team

3D Fokker-Planck Calculations of Electron and Ion Distributions in Tokamak Plasmas

3D Fokker-Planck Calculations of Electron and Ion Distributions in Tokamak Plasmas

M.R. O'Brien[1], M. Cox[1], C.D. Warrick[1], F.S. Zaitsev[2]
and JET Team*

JET-Joint Undertaking, Culham Science Centre, OX14 3DB, Abingdon, UK

[1]AEA Fusion (UKAEA/Euratom Fusion Association), Culham Laboratory, Abingdon, UK
[2]Moscow State University, Russia
** See Annex*

Preprint of a paper to be presented to IAEA Technical Committee Meeting on Advances in Simulation and Modelling Thermonuclear Plasmas (Montreal, 15-18 June 1992)

3D Fokker-Planck Calculations of Electron and Ion Distributions in Tokamak Plasmas

M R O'Brien, M Cox, C D Warrick and †F S Zaitsev

AEA Fusion, Culham Laboratory, Abingdon, UK
(UKAEA/Euratom Fusion Association)

†Moscow State University, Russia

ABSTRACT. Two 3D Fokker-Planck codes which calculate distribution functions in velocity and real space allowing for particle trapping, collisions, heating and radial transport in axisymmetric tokamaks, are described. The first, BANDIT-3D, is mainly used for calculating the influence of RF heating on the electron distribution and uses a two stage operator splitting algorithm. The second, FPP-3D, is currently being developed and uses a two cycle, six stage operator splitting algorithm to solve for neoclassical particle distributions. These algorithms are found to be efficient and robust allowing solution of 3D Fokker-Planck equations in modest CPU times on both a CRAY-2 supercomputer and high performance workstations.

1 Introduction

Fokker-Planck codes are widely used in modelling the effects of radio-frequency (RF) and other heating on electron and ion distribution functions in tokamaks and other fusion plasmas. Until recently, these codes have mainly solved the two dimensional Fokker-Planck problem, solving for the distribution f as a function of two velocity space coordinates as well as time [e.g. 1,2,3]. While these codes can model distortions in velocity space for a particular spatial location (flux surface in a tokamak), spatial transport processes have been largely ignored. This can be a serious shortcoming for modelling RF current drive in tokamaks for example, since even modest levels of radial transport can broaden the driven current profile significantly [4]. More recently however, three dimensional Fokker-Planck codes have been written [5,6,7,8], which solve for $f(v, \theta, r)$ (with v speed, θ pitch-angle and r flux surface radius), which include radial transport in the equation solved. These codes can solve both kinetic and transport problems simultaneously, with the quantities determined by ordinary transport codes (density, temperature, current density, etc.) given by velocity space moments of the calculated distribution function. In this paper we describe the numerical methods used in two such codes.

The first code, BANDIT-3D [6], discussed in section 2, solves the 3D electron Fokker-Planck equation for an arbitrarily shaped axisymmetric low collisionality tokamak, with the effects of collisions, RF and Ohmic heating, radial transport through an ad hoc diffusion plus convection term, and electron trapping all included. Details of the operators used to model the various effects are given elsewhere [3,6,9]: here we concentrate on the numerical method used to solve the equation. The code has recently been enhanced to allow treatment of

ion distributions for the study of ion cyclotron resonant heating (ICRH) and neutral beam heating: this has required only minor changes to the numerical approach adopted.

The second code, FPP-3D, described in section 3, has been written and is currently being tested. It solves a 3D Fokker-Planck equation for either ions or electrons with the radial operator that due to neoclassical transport. A particularly important feature of the treatment is that the transport (and other collisional) coefficients are calculated not as averages over flux surfaces, but as averages over drift surfaces (i.e. trajectories). This means that situations in which fast ion orbits do not closely follow flux surfaces (e.g. minority ions heated by ICRH in JET [10]) can be modelled and the neoclassical effects associated with both their non-Maxwellian distributions and their large orbit widths (e.g. transport and bootstrap currents) can be treated. The derivation of the 3D Fokker-Planck equation will not be described here, but has been submitted elsewhere [11].

2 BANDIT-3D

2.1 3D Electron Fokker-Planck Equation

BANDIT-3D solves the following bounce-averaged Fokker-Planck equation for the electron distribution function $f(\theta_o, v, r; t)$, with θ_o the pitch-angle on the outside of the flux surface whose radius in the equatorial plane is r, and v the relativistic momentum divided by the rest mass:

$$\frac{\partial f}{\partial t} = \frac{1}{v^2}\frac{\partial}{\partial v}\left[v^2 S^v\right] + \frac{1}{g\sin\theta_o}\frac{\partial}{\partial \theta_o}\left[g\sin\theta_o S^{\theta_o}\right] + \frac{1}{g(1+\epsilon)r}\frac{\partial}{\partial r}\left[rS^r\right] \tag{1}$$

with

$$S^{\theta_o} = S^{\theta_o\theta_o}\frac{\partial f}{\partial \theta_o} + S^{\theta_o v}\frac{\partial f}{\partial v} + S^{\theta_o f} f \tag{2}$$

$$S^v = S^{vv}\frac{\partial f}{\partial v} + S^{v\theta_o}\frac{\partial f}{\partial \theta_o} + S^{vf} f \tag{3}$$

$$S^r = S^{rr}\frac{\partial (g(1+\epsilon)f)}{\partial r} + S^{rf} g(1+\epsilon) f \tag{4}$$

In eq(1) $g(\theta_o, r) = \oint(\cos\theta_o/\cos\theta)ds/\oint ds$ with $\oint ds$ a field line integral for the flux surface of radius r, restricted for trapped electrons to accessible values of s, θ the pitch angle at field line position s, and $\epsilon = r/R_o$ the inverse aspect ratio of the flux surface. (For simplicity, eq(1) is written for circular surfaces but generalises readily to the non-circular equilibria treated by the code, which need not be up-down symmetric allowing study of single null X-point plasmas for example.) Equation (1) is in the form of the divergence of a flux in phase space to which several processes contribute. Electron-ion collisions are with background ion Maxwellians giving mainly pitch-angle scattering ($S^{\theta_o\theta_o}$). Electron-electron collisions, which contribute to all the diffusion and convection coefficients in velocity (θ_o, v) space, are calculated from the non-linear collision operator using the method described by Killeen et al. [3]. Ohmic heating contributes to the convective coefficients $S^{\theta_o f}$ and S^{vf}.

The code has a range of options for modelling RF (Electron Cyclotron Resonance, Lower Hybrid and low frequency Fast Wave) heating [9,12]: these are all based on quasilinear diffusion theories and give velocity space diffusion. One of these options, in which the RF diffusion coefficients are calculated from ray tracing data, is available for both ECRH and LH and merits a more detailed discussion. The launched RF spectrum is modelled by a bundle of rays (typically up to 50) which are each followed (perhaps for many reflections) by solving the ray tracing equations [e.g 13], and at each step on each ray parameters such as the wave polarisation, $k_{\|}$ and $\Delta k_{\|}$ are stored. Then, following an approach due to Harvey [14], RF diffusion coefficients are constructed in velocity space for each flux surface radius from these ray data. The Fokker-Planck calculation proceeds and as the distribution changes the RF diffusion coefficients at each ray step are adjusted to be consistent with a calculation of the damping along each ray.

Since there is no single accepted mechanism for the anomalously high radial transport of electrons observed in tokamaks, the radial diffusivity ($D_r = S^{rr}$) and pinch speed ($V_r = S^{rf}$) are not based on a particular model but are input by the user. They may be functions of all four variables $(\theta_o, v, r; t)$ although a convenient choice often used gives D_r and V_r only radial dependence with $D_r(dn/dr) + V_r n = 0$: this maintains a constant (in time) density profile.

2.2 BANDIT-3D: Numerical Method

The numerical method for solving eq(1) is summarised in this section: a more detailed description is given in reference [6]. A conservative, finite difference, two-stage operator splitting algorithm [5,15] is used to time advance the distribution at each point on a (usually, but not necessarily, uniform) (θ_o, v, r) mesh. (A fully implicit method, while giving a steady state solution after only one time-step if collisions are not updated, would have prohibitive memory and CPU requirements.) The finite differencing is centred except for the convective term involving $S^{vf}f$ which is partially upwinded for better treatment of the exponential drop of f with increasing v for Maxwellians [16]. In the first stage of the splitting algorithm, the velocity space (θ_o and v) components of eq(1) are advanced together: this advancement is implicit and therefore stable for arbitrary time-step Δt, allowing large Δt if only the steady state solution is required. The resulting matrix equations (one for each value of r) are solved by Gaussian elimination. Then in the second stage of the operator splitting, the radial transport operator is advanced implicitly: since there are no mixed (r,θ_o) and (r,v) derivatives in eq(1) this stage requires only a (very rapid) tridiagonal inversion. This means that 3D time dependent solutions require similar CPU times to 2D time dependent calculations (which of course omit transport) for the same number of flux surfaces, although steady-state calculations are generally quicker for the 2D problem. For rapid calculation of steady state solutions, an algorithm which uses the average of two previous distributions as input to the time-advancement has been found useful [6].

The boundary conditions used are (i) zero flux at $v = 0$, $\theta_o = 0 = \pi$ and $r = 0$; (ii) either zero flux or the "runaway" boundary condition discussed by Karney [1] at large v (typically $\sim 10 v_{th}$ with v_{th} the characteristic thermal speed $(2T_e/m_e)^{\frac{1}{2}}$ at the centre); (iii) a fixed in time, usually Maxwellian, distribution at $r = a$ with a the minor radius. Generally, the initial distribution is taken to be Maxwellian with specified density and temperature profiles. There are two classes of electron that must be represented by $f(\theta_o, v, r)$: those trapped in the non-uniform magnetic field of the tokamak (with $\theta_{TP} \leq \theta_o \leq \pi - \theta_{TP}$) and those not, the passing electrons. To model these correctly, we ensure both that f is continuous at the

trapped/passing boundaries (TPBs), and that the net flux of particles entering the TPB from the trapped and co- and counter-passing regions is zero. This is done in the first stage of the splitting by inserting, at the co- and counter-TPBs, two extra θ_o points at each radius, and using the appropriate flux-conservation equation [3]. For further details of how the TPBs are treated in a conservative manner see reference [6].

Velocity space moments of $f(\theta_o, v, r)$ yield the profiles $n_e(r)$, $T_e(r)$ and $j(r)$ (for example, $n_e(r) = 2\pi(1+\epsilon)\int_0^\infty v^2 dv \int_0^\pi g(\theta_o, r)\sin\theta_o \; f(\theta_o, v, r) \; d\theta_o$ for circular flux surfaces). In addition, Electron Cyclotron Emission and Bremsstrahlung spectra may be calculated from the 3D distributions calculated allowing further comparison with experimental data. The sequence of calculations in a typical BANDIT-3D run is as follows.

1. Set up stage including specification of (optionally non-circular) equilibrium, calculation of mesh parameters, etc., initialisation of collision and transport operators.
2. If required, calculate ray trajectories for ECRH or LH heating and store ray data.
3. Initialise diffusive coefficients arising from RF heating.
4. Advance distribution one time-step in two stages.
5. Calculate density, temperature and current profiles as velocity space integrals of f.
6. If maximum number of time-steps has been reached or a convergence criterion satisfied then optionally calculate ECE and Bremsstrahlung spectra and plot profiles and distributions. Otherwise repeat steps 4 and 5, recalculating collision operator and updating RF diffusion coefficients if required.

BANDIT-3D runs on a CRAY-2 mainframe and Unix workstations. On the CRAY-2 it takes $\sim$ 5 CPU minutes for a (80,100,20) (θ_o,v,r) mesh for 20 time-steps (although often less than 10 steps are required to reach steady state) although runs with ray tracing can take longer. The code is often run with smaller meshes on an IBM-6000 RISC workstation, requiring $\sim$ 15 CPU minutes for 20 time-steps and a (40,80,20) mesh. For big meshes the time taken is determined by the Gaussian eliminator and scales as $N_{\theta_o}^2 N_v N_r$ per time-step. The eliminator requires a large array for the velocity space step matrix inversion ($\sim 3N_{\theta_o}^2 N_v$ words) and so dominates the memory requirements of large problems (although these are still within the capabilities of modern large memory workstations for all but the biggest problems).

2.3 BANDIT-3D: Examples of Use

The principle use of BANDIT-3D is to study the influence of radial transport on kinetic effects in tokamaks. As an illustration, Figure 1 shows calculated profiles for planned experiments in the COMPASS-D tokamak in which the effects of localised ECRH current drive (ECCD) on $m/n = 2/1$ MHD activity will be studied. A number of authors (e.g. [17]) have suggested that localised current drive close to a rational surface might be used to suppress tearing activity in tokamaks, and indeed the use of ECCD for this purpose has been proposed for ITER. In Figure 1, a combined ray tracing/Fokker-Planck calculation shows that, if radial transport effects are neglected (and BANDIT-3D is run as a 2D Fokker-Planck code for several flux surfaces), very localised current profiles are calculated. However if a level of transport comparable to the bulk thermal conductivity and independent of θ_o and v is

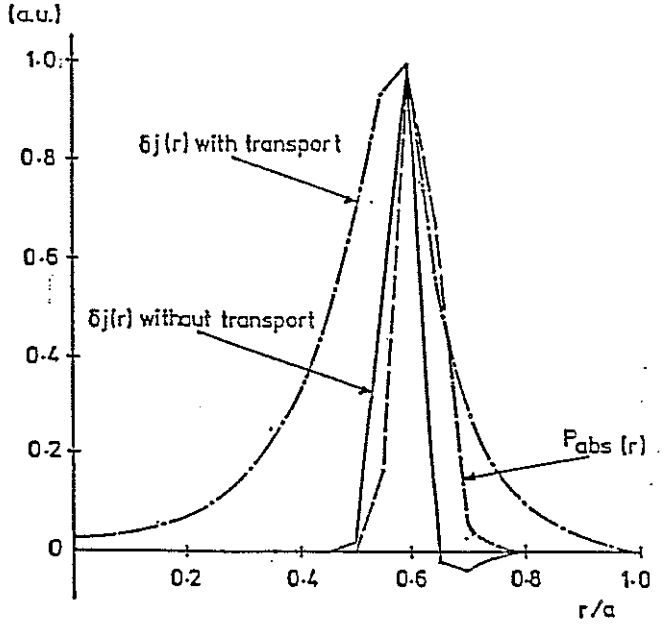

Figure 1 Absorption profile ($P_{abs}(r)$) and driven current profiles ($\delta j(r)$) with and without transport for planned 60GHz X mode second harmonic ECCD mode stabilisation experiments in COMPASS-D ($R_o = 0.56$m, $a = 0.2$m, $\kappa = 1.5$, $B_o = 0.82$T) . All profiles are normalised to their peak values. Parabolic density and temperature profiles ($n_e(0) = 1.7 \times 10^{19}\mathrm{m}^{-3}$, $n_e(a) = 0.17 \times 10^{19}\mathrm{m}^{-3}$, $T_{eo} = 1.5$keV) and $Z_{eff} = 2$ were assumed. The power was launched from the outside equatorial plane at an angle 13° to the major radius, and absorption was to the high field side of the magnetic axis. With transport ($n_e(r)D_r(r) = 5 \times 10^{19}\mathrm{m}^{-1}\mathrm{s}^{-1}$) $\delta j(r)$ is significantly broader than without, although the calculated ECCD efficiency (0.06A/W) is the same for both cases.

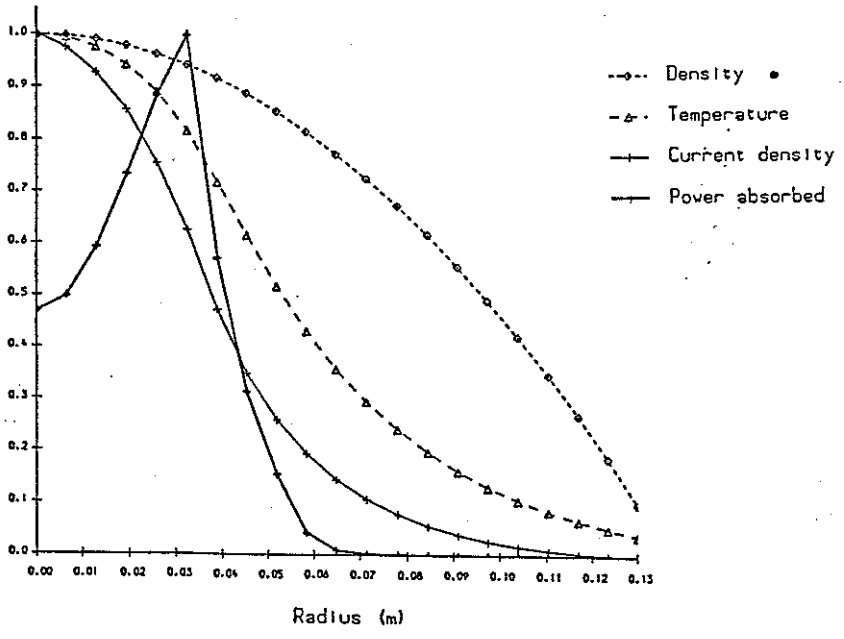

Figure 2 Profiles predicted by BANDIT-3D for an ECCD discharge in CLEO ($R_o = 0.9$m, $a = 0.13$m, $B_o = 1$T). 150kW of 60GHz X mode second harmonic ECRH power drove $\sim$ 4kA of the plasma current (10kA) with the remainder driven by the loop Voltage (0.15V). $n_e(r)$ and $T_e(r)$ are normalised to $6 \times 10^{19}\mathrm{m}^{-3}$ and 1.3keV. The absorbed power is normalised to 5.0MW m^{-3} and $j(r)$ to 5.8MA m^{-2}. The radial transport chosen ($n_e(r)D_r(r) = 1.5(1 + 3(r/a)^3) \times 10^{19}\mathrm{m}^{-1}\mathrm{s}^{-1}$, with V_r taken to maintain a given $n_e(r)$) gave both the correct total current and the observed temperature

assumed, the driven current profile $\delta j(r)$ is broadened significantly, even though the total current driven is little changed. The resulting efficiency and current profile width should still be adequate for mode control experiments, however.

In these calculations, the radial transport was chosen to maintain the given density profile, and the collisions were not energy conserving and so kept the temperature profile close to that specified. It is possible however to run with the full particle, momentum and energy conserving collision operator in which case BANDIT-3D runs as a combined kinetic/transport code and the temperature profile evolves to give a consistent balance between the heating and transport terms. For example, Figure 2 shows the calculated plasma profiles for ECCD experiments on the CLEO tokamak in which radial transport was deduced to play an important role. The temperature and current profiles were consistent with experiment showing that the level of radial transport chosen could account for both the observed temperature profile and the observed driven current, which was less than that predicted by theories which neglected radial transport. For more details of this simulation see reference [9].

3 FPP-3D

The neoclassical theory of plasma transport has generally been restricted to particle distributions close to Maxwellian and to particles slow enough that their trajectories closely follow flux surfaces. We have developed a code FPP-3D which solves for either the electron or ion distribution function, which need not be close to Maxwellian, without the assumption of trajectories close to flux surfaces and using the full collision operator which yields neoclassical radial transport. In tokamak experiments, fast ions appear to slow down and be transported classically [e.g. 18], justifying the study of neoclassical transport of non-Maxwellian fast ions, in particular of alpha particles and ICRH generated hot ions, allowed by FPP-3D.

The equation solved, a full derivation of which is described elsewhere [11], is

$$\frac{\partial f}{\partial t} = \frac{v_c^3}{\tau_c} \sum_{n=1,2,3} \frac{1}{\langle 1 \rangle} \frac{\partial}{\partial x_n} \left[\sum_{m,i,k,\beta} \frac{\partial f}{\partial x_m} \langle \frac{\partial x_n}{\partial v_i} \frac{\partial x_m}{\partial v_k} a_\beta^{ik}(f_\beta) \rangle + f \langle \frac{\partial x_n}{\partial v_i} b_\beta^i(f_\beta) \rangle \right] \qquad (5)$$

(Derivation of operators for other effects (for example, additional heating and magnetic ripple) using the method described in [11] is underway: the resulting equations will be of the same form as eq(5) and amenable to the numerical algorithm discussed here.) In eq(5) the distribution f is a function of time and three constants of the unperturbed motion $x = (x_1, x_2, x_3) = (\theta_o, v_o, r_o)$, where θ_o is the pitch-angle on the outermost point of the trajectory (outside leg of the banana orbit for trapped particles), v_o is the generalised speed including the electrostatic potential ($\sqrt{v^2 + q\Phi}$), and r_o is the flux surface radius at the point on the trajectory where the magnetic field is maximum (banana tip for trapped particles). The coefficients a_β^{ik} and b_β^i are from collisions with particle species β, v_c and τ_c are a characteristic speed and collision time and v_i ($i = 1...3$) are Cartesian velocity space coordinates. Locally, collisions change only velocity space coordinates v_i, however transformation to the constants of motion system x_n leads to a flux in both the velocity-space-like variables θ_o and v_o and in the real space variable r_o. Angular brackets $\langle ... \rangle$ represent a Jacobian weighted trajectory (not flux surface) average over poloidal angle [11].

Equation (5) is of the same basic structure as eq(1) and, we use a conservative finite dif-

ference scheme and boundary conditions at the extrema of θ_o, v_o and r_o similar to those in BANDIT-3D. Also, f is continuous at the trapped/passing boundary (TPB) as in BANDIT-3D. However, solution of this equation requires a more sophisticated algorithm than that used in BANDIT-3D in several respects. Firstly, calculation of the collisional coefficients in eq(5) requires evaluation of a four dimensional integral (3 velocity space coordinates plus poloidal angle, without the assumption of constant flux surface radius) for each set of three constants of the motion (θ_o, v_o, r_o). This is reduced to $O(N^5)$ operations by using gyroangle-independence and a Legendre expansion for the distribution functions [cf. 3]. Secondly, the TPB condition, while still a flux conservation equation [11], is much more complicated than for BANDIT-3D, and a non-uniform θ_o mesh with points either side of, but not actually at, the TPB for each radial point is found more suitable than the grid used in BANDIT-3D. Thirdly, the presence of mixed (θ_o, r_o) and (v_o, r_o) derivatives requires a more involved time-advancement algorithm which is now described.

A two cycle, six stage operator splitting scheme is employed. This has attractive stability properties for positive definite linear problems [19], and is second order accurate in time, although for weakly non-linear problems which may not be positive definite, as here, these properties have not been rigorously proved. With $1, 2, 3$ representing θ_o, v_o and r_o respectively, we approximate eq(5) as

$$\frac{\partial f}{\partial t} = \Lambda f$$

with

$$\Lambda = \Lambda_{11} + \Lambda_{12} + \Lambda_{13} + \Lambda_{21} + \Lambda_{22} + \Lambda_{23} + \Lambda_{31} + \Lambda_{32} + \Lambda_{33}$$

Here the θ_o component, for example, of the divergence of the flux in eq(5) is split into Λ_{12} and Λ_{13} (the mixed derivative parts) and Λ_{11} (the remainder). We then split Λ into three operators, $\Lambda = \Lambda_1 + \Lambda_2 + \Lambda_3$, where

$$\Lambda_1 = \mu_1\Lambda_{11} + \mu_2\Lambda_{22} + \Lambda_{12} + \Lambda_{21}$$

$$\Lambda_2 = (1-\mu_2)\Lambda_{22} + \mu_3\Lambda_{33} + \Lambda_{23} + \Lambda_{32}$$

$$\Lambda_3 = (1-\mu_1)\Lambda_{11} + (1-\mu_3)\Lambda_{33} + \Lambda_{13} + \Lambda_{31}$$

with μ_k weights, typically 0.5. The two cycle algorithm for advancement from the (n-1)th to the (n+1)th time step proceeds as follows:

$$\frac{f^{n-2/3} - f^{n-1}}{\tau} = \Lambda_1^n \left(\lambda_1 f^{n-2/3} + (1-\lambda_1) f^{n-1}\right)$$

$$\frac{f^{n-1/3} - f^{n-2/3}}{\tau} = \Lambda_2^n \left(\lambda_2 f^{n-1/3} + (1-\lambda_2) f^{n-2/3}\right)$$

$$\frac{f^{n} - f^{n-1/3}}{\tau} = \Lambda_3^n \left(\lambda_3 f^{n} + (1-\lambda_3) f^{n-1/3}\right)$$

$$\frac{f^{n+1/3} - f^{n}}{\tau} = \Lambda_3^n \left(\lambda_3 f^{n+1/3} + (1-\lambda_3) f^{n}\right)$$

$$\frac{f^{n+2/3} - f^{n+1/3}}{\tau} = \Lambda_2^n \left(\lambda_2 f^{n+2/3} + (1-\lambda_2) f^{n+1/3}\right)$$

$$\frac{f^{n+1} - f^{n+2/3}}{\tau} = \Lambda_1^n \left(\lambda_1 f^{n+1} + (1-\lambda_1) f^{n+2/3}\right)$$

$$\Lambda_k^n = \Lambda_k(t_n, \tilde{f}^n), \quad k = 1,2,3$$

with λ_k implicitness weights, $\tau = t_n - t_{n-1}$ and $\tilde{f}^n$, which affects the collisional coefficients in Λ_k^n, from the explicit step

$$\tilde{f}^n = f^{n-1} + \tau\Lambda(t_{n-1}, f^{n-1}) f^{n-1}$$

At each stage a 2D implicit (or semi-implicit) operator is inverted by Gaussian elimination of a sparse banded matrix. Thus the mixed (and other) derivatives are always advanced implicitly allowing large time-steps while maintaining stability. For the first stage this algorithm requires $O(N_{r_o} N_{v_o} (N_{\theta_o})^2)$ operations (the bandwidth is $O(N_{\theta_o})$). The CPU time for time advancement is dominated by the first and last stages because for other stages the bandwidth of the matrix is $O(N_{r_o})$ and usually $N_{r_o} < N_{\theta_o} < N_{v_o}$.

This algorithm has proved robust with steady state solutions obtained in modest numbers of full time-steps (typically $\sim$ 20). FPP-3D runs on both a CRAY-2 and an IBM-6000 RISC workstation. CPU times and memory requirements depend greatly on the mesh size employed and tend to be dominated by the initial calculation of the collisional coefficients, with later updating of coefficients more rapid. Large work arrays required for the calculation of these coefficients are written to and read from disk to reduce memory requirements. A typical CRAY-2 run with $(N_{\theta_o}, N_{v_o}, N_{r_o}) = (60, 80, 20)$ takes $\sim$ 5 minutes of CPU time, whereas on the workstation a (30,22,5) grid takes $\sim$ 15 minutes. The code is presently being tested by comparing calculated currents and particle and energy fluxes with those derived analytically for distributions close to Maxwellian and for trajectories close to flux surfaces [20]. A simplified version of eq(5), containing only the neoclassical radial diffusion coefficient, has already been solved numerically [21], with results consistent with analytic results and with 2D calculations.

One use of FPP-3D will be to compare neoclassical fluxes with the collisional coefficients calculated as flux surface averages and as trajectory averages. Figure 3 shows JD_{rr} the product of the Jacobian and the radial diffusivity for hydrogen ions with energies $\leq$ 10MeV in a circular JET-sized plasma with $R = 3$m, $a = 1.2$m, $B_o = 2$T and $I_P = 1$MA, conditions appropriate to minority ICRH experiments. The ions collide with electron and Deuterium Maxwellians (parabolic $n(r)$ with $n_o = 10^{20}\text{m}^{-3}$ and parabolic squared $T(r)$ with $T_o =$ 10keV). Contouring is as a function of v_o and θ_o for $r_o = 0.4$a for averaging over surfaces (Figure 3(a)) and over trajectories (Figure 3(b)). Since the radial diffusivity varies $\sim 1/v_0$ and the Jacobian varies $\sim v_0^2$, JD_{rr} increases $\sim$ linearly with speed v_0. It is almost zero for passing particles except those close to the TPB and peaks at the TPB in Figure 3, both properties as expected for neoclassical transport. Both the magnitude and v_o, θ_o variation differ for the two cases showing the importance of averaging over trajectories rather than flux surfaces when calculating transport coefficients for fast ions.

4 Summary

The two codes described in this paper, BANDIT-3D and FPP-3D, allow solution of a wide range of kinetic and transport problems in non-circular tokamaks. A variety of heating

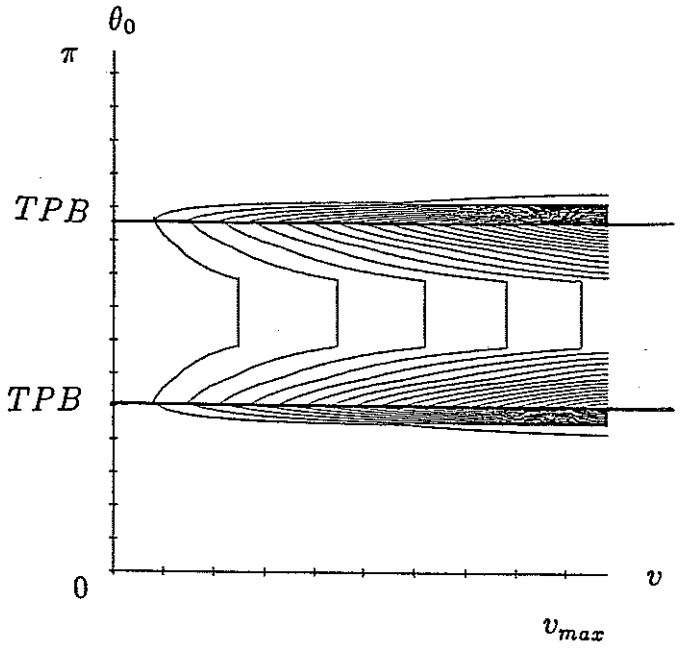

Figure 3(a) The product of the Jacobian and the neoclassical radial diffusion coefficient (JD_{rr}) calculated as a flux surface average and plotted against speed and pitch-angle for $r = 0.4a$ for Hydrogen ions in a circular JET-sized plasma ($R = 3$m, $a = 1.2$m, $B_o = 2$T, $I_P = 1$MA). The maximum speed corresponds to an energy of 10MeV and the values of θ_o at the trapped/passing boundary (TPB) are indicated. The ions collide with background electrons and Deuterium ions (parabolic $n(r)$ with $n_o = 10^{20}\text{m}^{-3}$ and parabolic squared $T(r)$ with $T_o = 10$keV), conditions appropriate to minority ICRH experiments in JET.

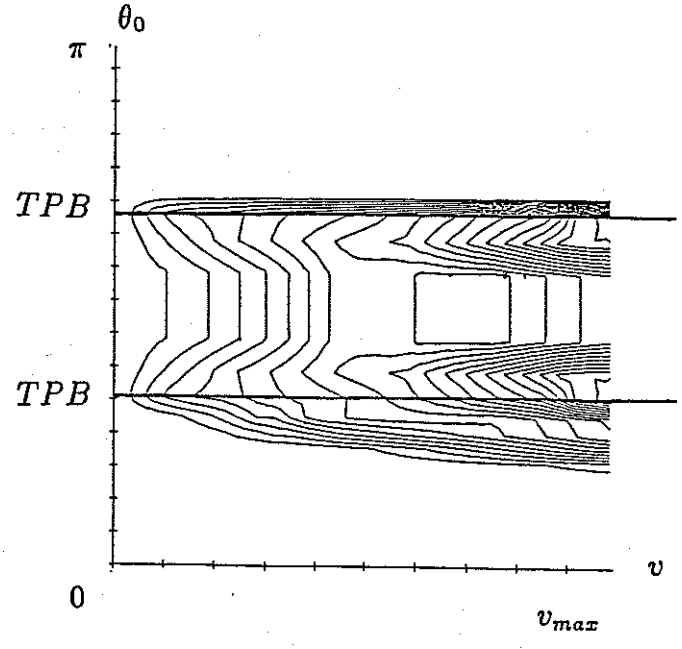

Figure 3(b) As Figure 3(a) but with JD_{rr} calculated as a trajectory average, showing the importance of averaging over drift orbits for fast ions. Note that JD_{rr} is symmetric, for a given v, in the trapped region, but asymmetric in the passing regions unlike Figure 3(a).

options is available in the BANDIT-3D code, including for ECRH and LH the option of a self-consistent ray tracing/Fokker-Planck/transport calculation. The FPP-3D code includes the full neoclassical collision/transport operator, without the assumption that drift orbits are close to flux surfaces: this should prove particularly useful in the study of fast ions (especially alpha particles) in next generation tokamaks such as ITER. The conservative, finite difference algorithms used, which give consistent treatment of the trapped/passing boundary, have proved robust and efficient and allow solution on both CRAY supercomputers and high performance workstations in modest CPU times.

ACKNOWLEDGEMENTS. The authors are grateful to M G McCoy (N.E.R.S.C., Lawrence Livermore National Laboratory, California) for use of the collision package and Gaussian eliminator from the CQL-3D code in BANDIT-3D, to R W Harvey (General Atomics, San Diego) for useful discussions concerning implementing ray tracing data in Fokker-Planck codes, and to D P Kostomarov (Moscow State University) for helpful discussions on numerical methods. The BANDIT-3D code was developed in part for a Task Agreement with the JET Joint Undertaking.

REFERENCES.

[1] Karney, C.F.F., Comp. Phys. 4 (1986) 183.
[2] O'Brien, M.R., Cox M., Start D.F.H., Nucl. Fusion **26** (1986) 1625.
[3] Killeen, J., Kerbel, G.D., McCoy, M.G., Mirin, A.A., Computational Methods for Kinetic Models of Magnetically Confined Plasmas, Springer-Verlag, New York (1986).
[4] Dendy R.O., O'Brien, M.R., Nucl. Fusion **31** (1991) 583.
[5] Hammett G.W., Fast Ion Studies of Ion Cyclotron Heating in the PLT Tokamak, Ph.D Dissertation, Princeton University (1986).
[6] McKenzie J.S., O'Brien, M.R., Cox, M., Comp. Phys. Commun. **66** (1991) 194.
[7] Fukuyama, A., Ueeda, T., in Controlled Fusion and Plasma Physics, (Proc. 17th Eur. Conf. Amsterdam, 1990), Vol. III, European Physical Society (1990) 1251.
[8] Giruzzi, G., in Proc. of IAEA Technical Committee Meeting on Fast Wave Current Drive in Reactor Scale Tokamaks, Arles 1991, 76.
[9] O'Brien, M.R., Cox M., McKenzie, J.S., Warrick, C.D., in Controlled Fusion and Plasma Physics, (Proc. 18th Eur. Conf. Berlin, 1991), Part III, European Physical Society (1991) 261.
[10] Start D. F. H. and the JET Team, 13th International Conference on Plasma Physics and Controlled Nuclear Fusion Research, Washington, 1990, IAEA, Vienna (1991), Vol 1 679.
[11] F S Zaitsev, M R O'Brien and M Cox, submitted to Phys. Fluids B.
[12] Cox, M., O'Brien, M.R. and Warrick, C.D., in Proc. of IAEA Technical Committee Meeting on Fast Wave Current Drive in Reactor Scale Tokamaks, Arles 1991, 122.
[13] Bonoli, P., Englade, R.C., Phys. Fluids, **29** (1986) 2937.
[14] Harvey, R.W., private communication. See the paper by Harvey et al. in these proceedings.
[15] Richtmyer, R.D., Morton, K.W., Difference Methods for Initial-Value Problems, Interscience, New York (1967).
[16] Chang, J.S., Cooper, G.J., Comput. Phys. **6** (1970) 1.
[17] Westerhof, E., Nucl. Fusion, **30** (1990) 1143.
[18] Heidbrink, W.W., Barnes, C.W., Hammett, G.W., et al., Phys. Fluids B **3** (1991) 3167.
[19] Marchuk, G.I., Methods of Numerical Mathematics, Springer-Verlag, New York, second edition, (1982), especially pages 243-253.
[20] Hinton, F.L., Hazeltine, R.D., Reviews of Modern Physics **48** (1976) 239.
[21] Zaitsev, F.S., Smirnov, A.P., O'Brien, M.R., Cox, M., in Controlled Fusion and Plasma Physics, (Proc. 18th Eur. Conf. Berlin, 1991), Part IV, European Physical Society (1991) 145.

ANNEX

P.-H. REBUT, A. GIBSON, M. HUGUET, J.M. ADAMS[1], B. ALPER, H. ALTMANN, A. ANDERSEN[2], P. ANDREW[3], M. ANGELONE[4], S. ALI-ARSHAD, P. BAIGGER, W. BAILEY, B. BALET, P. BARABASCHI, P. BARKER, R. BARNSLEY[5], M. BARONIAN, D.V. BARTLETT, L. BAYLOR[6], A.C. BELL, G. BENALI, P. BERTOLDI, E. BERTOLINI, V. BHATNAGAR, A.J. BICKLEY, D. BINDER, H. BINDSLEV[2], T. BONICELLI, S.J. BOOTH, G. BOSIA, M. BOTMAN, D. BOUCHER, P. BOUCQUEY, P. BREGER, H. BRELEN, H. BRINKSCHULTE, D. BROOKS, A. BROWN, T. BROWN, M. BRUSATI, S. BRYAN, J. BRZOZOWSKI[7], R. BUCHSE[22], T. BUDD, M. BURES, T. BUSINARO, P. BUTCHER, H. BUTTGEREIT, C. CALDWELL-NICHOLS, D.J. CAMPBELL, P. CARD, G. CELENTANO, C.D. CHALLIS, A.V. CHANKIN[8], A. CHERUBINI, D. CHIRON, J. CHRISTIANSEN, P. CHUILON, R. CLAESEN, S. CLEMENT, E. CLIPSHAM, J.P. COAD, I.H. COFFEY[9], A. COLTON, M. COMISKEY[10], S. CONROY, M. COOKE, D. COOPER, S. COOPER, J.G. CORDEY, W. CORE, G. CORRIGAN, S. CORTI, A.E. COSTLEY, G. COTTRELL, M. COX[11], P. CRIPWELL[12], O. Da COSTA, J. DAVIES, N. DAVIES, H. de BLANK, H. de ESCH, L. de KOCK, E. DEKSNIS, F. DELVART, G.B. DENNE-HINNOV, G. DESCHAMPS, W.J. DICKSON[13], K.J. DIETZ, S.L. DMITRENKO, M. DMITRIEVA[14], J. DOBBING, A. DOGLIO, N. DOLGETTA, S.E. DORLING. P.G. DOYLE, D.F. DÜCHS, H. DUQUENOY, A. EDWARDS, J. EHRENBERG, A. EKEDAHL, T. ELEVANT[7], S.K. ERENTS[11], L.G. ERIKSSON, H. FAJEMIROKUN[12], H. FALTER, J. FREILING[15], F. FREVILLE, C. FROGER, P. FROISSARD, K. FULLARD, M. GADEBERG, A. GALETSAS, T. GALLAGHER, D. GAMBIER, M. GARRIBBA, P. GAZE, R. GIANNELLA, R.D. GILL, A GIRARD, A. GONDHALEKAR, D. GOODALL[11], C. GORMEZANO, N.A. GOTTARDI, C. GOWERS, B.J. GREEN, B. GRIEVSON, R. HAANGE, A. HAIGH, C.J. HANCOCK, P.J. HARBOUR, T. HARTRAMPF, N.C. HAWKES[11], P. HAYNES[11], J.L. HEMMERICH, T. HENDER[11], J. HOEKZEMA, D. HOLLAND, M. HONE, L. HORTON, J. HOW, M. HUART, I. HUGHES, T.P. HUGHES[10], M. HUGON, Y. HUO[16], K. IDA[17], B. INGRAM, M. IRVING, J. JACQUINOT, H. JAECKEL, J.F. JAEGER, G. JANESCHITZ, Z. JANKOVICZ[18], O.N. JARVIS, F. JENSEN, E.M. JONES, H.D. JONES, L.P.D.F. JONES, S. JONES[19], T.T.C. JONES, J.-F. JUNGER, F. JUNIQUE, A. KAYE, B.E. KEEN, M. KEILHACKER, G.J. KELLY, W. KERNER, A. KHUDOLEEV[21], R. KONIG, A. KONSTANTELLOS, M. KOVANEN[20], G. KRAMER[15], P. KUPSCHUS, R. LÄSSER, J.R. LAST, B. LAUNDY, L. LAURO-TARONI, M. LAVEYRY, K. LAWSON[11], M. LENNHOLM, J. LINGERTAT[22], R.N. LITUNOVSKI, A. LOARTE, R. LOBEL, P. LOMAS, M. LOUGHLIN, C. LOWRY, J. LUPO, A.C. MAAS[15], J. MACHUZAK[19], B. MACKLIN, G. MADDISON[11], C.F. MAGGI[23], G. MAGYAR, W. MANDL[22], V. MARCHESE, G. MARCON, F. MARCUS, J. MART, D. MARTIN, E. MARTIN, R. MARTIN-SOLIS[24], P. MASSMANN, G. MATTHEWS, H. McBRYAN, G. McCRACKEN[11], J. McKIVITT, P. MERIGUET, P. MIELE, A. MILLER, J. MILLS, S.F. MILLS, P. MILLWARD, P. MILVERTON, E. MINARDI[4], R. MOHANTI[25], P.L. MONDINO, D. MONTGOMERY[26], A. MONTVAI[27], P. MORGAN, H. MORSI, D. MUIR, G. MURPHY, R. MYRNÄS[28], F. NAVE[29], G. NEWBERT, M. NEWMAN, P. NIELSEN, P. NOLL, W. OBERT, D. O'BRIEN, J. ORCHARD, J. O'ROURKE, R. OSTROM, M. OTTAVIANI, M. PAIN, F. PAOLETTI, S. PAPASTERGIOU, W. PARSONS, D. PASINI, D. PATEL, A. PEACOCK, N. PEACOCK[11], R.J.M. PEARCE, D. PEARSON[12], J.F. PENG[16], R. PEPE DE SILVA, G. PERINIC, C. PERRY, M. PETROV[21], M.A. PICK, J. PLANCOULAINE, J.-P POFFÉ, R. PÖHLCHEN, F. PORCELLI, L. PORTE[13], R. PRENTICE, S. PUPPIN, S. PUTVINSKII[8], G. RADFORD[30], T. RAIMONDI, M.C. RAMOS DE ANDRADE, R. REICHLE, J. REID, S. RICHARDS, E. RIGHI, F. RIMINI, D. ROBINSON[11], A. ROLFE, R.T. ROSS, L. ROSSI, R. RUSS, P. RUTTER, H.C. SACK, G. SADLER, G. SAIBENE, J.L. SALANAVE, G. SANAZZARO, A. SANTAGIUSTINA, R. SARTORI, C. SBORCHIA, P. SCHILD, M. SCHMID, G. SCHMIDT[31], B. SCHUNKE, S.M. SCOTT, L. SERIO, A SIBLEY, R. SIMONINI, A.C.C. SIPS, P. SMEULDERS, R. SMITH, R. STAGG, M. STAMP, P. STANGEBY[3], R. STANKIEWICZ[32], D.F. START, C.A. STEED, D. STORK, P.E. STOTT, P. STUBBERFIELD, D. SUMMERS, H. SUMMERS[13], L. SVENSSON, J.A. TAGLE[33], M. TALBOT, A. TANGA, A. TARONI, C. TERELLA, A TERRINGTON, A TESINI, P.R. THOMAS, E. THOMPSON, K. THOMSEN, F. TIBONE, A. TISCORNIA, P. TREVALION, B. TUBBING, P. VAN BELLE, H. VAN DER BEKEN, G. VLASES, M. VON HELLERMANN, T. WADE, C. WALKER, R. WALTON[31], D. WARD, M.L. WATKINS, N. WATKINS, M.J. WATSON, S. WEBER[34], J. WESSON, T.J. WIJNANDS, J. WILKS, D. WILSON, T. WINKEL, R. WOLF, D. WONG, C. WOODWARD, Y. WU[35], M. WYKES, D. YOUNG, I.D. YOUNG, L. ZANNELLI, A. ZOLFAGHARI[19], W. ZWINGMANN

[1] Harwell Laboratory, UKAEA, Harwell, Didcot, Oxfordshire, UK.
[2] Risø National Laboratory, Roskilde, Denmark.
[3] Institute for Aerospace Studies, University of Toronto, Downsview, Ontario, Canada.
[4] ENEA Frascati Energy Research Centre, Frascati, Rome, Italy.
[5] University of Leicester, Leicester, UK.
[6] Oak Ridge National Laboratory, Oak Ridge, TN, USA.
[7] Royal Institute of Technology, Stockholm, Sweden.
[8] I.V. Kurchatov Institute of Atomic Energy, Moscow, Russian Federation.
[9] Queens University, Belfast, UK.
[10] University of Essex, Colchester, UK.
[11] Culham Laboratory, UKAEA, Abingdon, Oxfordshire, UK.
[12] Imperial College of Science, Technology and Medicine, University of London, London, UK.
[13] University of Strathclyde, Glasgow, UK.
[14] Keldysh Institute of Applied Mathematics, Moscow, Russian Federation.
[15] FOM-Institute for Plasma Physics "Rijnhuizen", Nieuwegein, Netherlands.
[16] Institute of Plasma Physics, Academia Sinica, Hefei, Anhui Province, China.
[17] National Institute for Fusion Science, Nagoya, Japan.
[18] Soltan Institute for Nuclear Studies, Otwock/Świerk, Poland.
[19] Plasma Fusion Center, Massachusetts Institute of Technology, Boston, MA, USA.
[20] Nuclear Engineering Laboratory, Lappeenranta University, Finland.
[21] A.F. Ioffe Physico-Technical Institute, St. Petersburg, Russian Federation.
[22] Max-Planck-Institut für Plasmaphysik, Garching, Germany.
[23] Department of Physics, University of Milan, Milan, Italy.
[24] Universidad Complutense de Madrid, Madrid, Spain.
[25] North Carolina State University, Raleigh, NC, USA.
[26] Dartmouth College, Hanover, NH, USA.
[27] Central Research Institute for Physics, Budapest, Hungary.
[28] University of Lund, Lund, Sweden.
[29] Laboratorio Nacional de Engenharia e Tecnologia Industrial, Sacavem, Portugal.
[30] Institute of Mathematics, University of Oxford, Oxford, UK.
[31] Princeton Plasma Physics Laboratory, Princeton University, Princeton, NJ, USA.
[32] RCC Cyfronet, Otwock/Świerk, Poland,
[33] Centro de Investigaciones Energéticas, Medioambientales y Tecnológicas, Madrid, Spain.
[34] Freie Universität, Berlin, Germany.
[35] Insitute for Mechanics, Academia Sinica, Beijing, China.